View metadata, citation and similar papers at core.ac.uk

brought to you by CORE

provided by HKU Scholars Hub

The HKU Scholars Hub The University of Hong Kong 香港大學學術庫

Title	Performance and cost comparison of permanent-magnet vernier machines
Author(s)	Li, J; Chau, KT
Citation	IEEE Transactions on Applied Superconductivity, 2012, v. 22 n. 3, p. 5202304:1-4
Issued Date	2012
URL	http://hdl.handle.net/10722/164045
Rights	Creative Commons: Attribution 3.0 Hong Kong License

Performance and Cost Comparison of Permanent-Magnet Vernier Machines

Jiangui Li, *Student Member, IEEE*, and K. T. Chau, *Senior Member, IEEE*

***Abstract*—This paper presents a quantitative comparison of two direct-drive outer-rotor permanent-magnet vernier (PMV) machines—namely the pole-splitting permanent-magnet vernier machine and vernier hybrid machine with emphasis on their performances and costs. The operating principles of two machines are discussed and their steady-state and transient performances are analyzed using the time-stepping finite element method. The overall weights and costs are also evaluated. The comparison results can be used to assess the validity of the designs of PMV machines.**

***Index Terms*—Direct-drive machine, finite element method, permanent-magnet machine, vernier machine.**

I. Introduction

CURRENTLY, in the applications like wind power generation, the mechanical gear is used to match the high rotational speed of conventional electric machines to low rotational speed of wind turbines. The mechanical gear causes wear and tear, audible noise and low efficiency, increased machine size, weight and material cost. The magnetic geared generator generally has cumbersome structure [1]. Recently, this matching problem has been solved by introducing the vernier effect (or magnetic gear effect) into a permanent-magnet (PM) machine, which is called the permanent-magnet vernier (PMV) machine [2].

There are mainly two types of PMV machines, classified according to the method of modulation. One type is called vernier hybrid (VH) machine, which uses the PMs on the stator to modulate the airgap magnetic field [3], [4]. The other type of PMV machine uses the slotted stator teeth to modulate the airgap magnetic field, called the pole-splitting permanent-magnet vernier (PSPMV) machine [5], [6]. The comparison of these two PMV machines has not been reported.

The purpose of this paper is to quantitatively compare two outer-rotor PMV machines for direct-drive applications, namely the PSPMV machine and VH machine. In Section II, the mathematical model will be presented. Section III will be devoted to the time-stepping finite element method analysis of the two PMV machines. The machine performances will be assessed, and hence quantitatively compared. Finally, conclusion will be drawn in Section IV.

Manuscript received September 12, 2011; accepted December 04, 2011. Date of publication December 15, 2011; date of current version May 24, 2012. This work was supported by the Research Grants Council, Hong Kong, under Grant HKU710711E.

The authors are with the Department of Electrical and Electronic Engineering, The University of Hong Kong, Hong Kong (e-mail: jgli@eee.hku.hk).

Color versions of one or more of the figures in this paper are available online at http://ieeexplore.ieee.org.

Digital Object Identifier 10.1109/TASC.2011.2180009

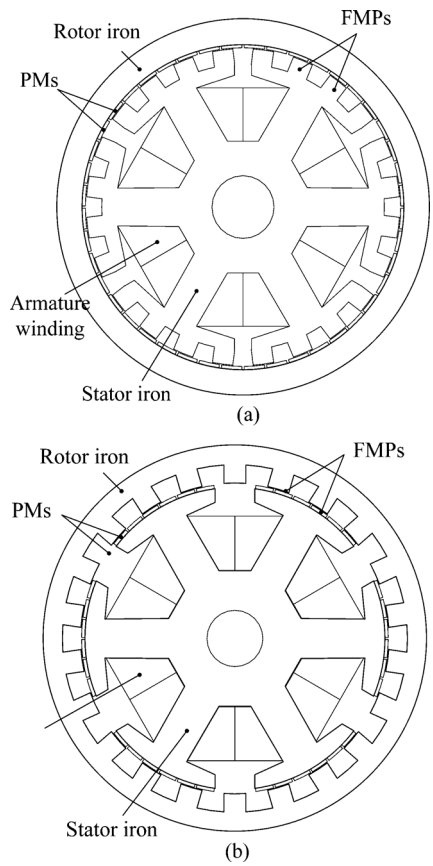

Fig. 1. Machine topologies. (a) PSPMV machine. (b) VH machine.

II. Machine Topologies

Fig. 1(a) shows the topology of the PSPMV machine. In the PSPMV machine design, there are 6 slots in the inner stator, which are occupied by 3-phase armature windings with 4 poles ($p_{\rm s} = 2$). Each stator tooth of PSPMV machine is split into 4 flux-modulation poles (FMPs), thus constituting totally 24 FMPs ($N_{\rm s} = 24$). According to the theory of vernier machines, the general relationship between the pole numbers and phase number is governed by:

$$p_r = N_s - p_s \tag{1}$$

where $N_{\rm s}$ is the number of FMPs, $p_{\rm r}$ is the number of rotor PM pole-pairs and $p_{\rm s}$ is the number of armature winding pole-pairs. From (1), $p_{\rm r} = 22$ is resulted, which denotes that there are 44 PM poles mounting on the outer rotor. In order to provide the

1051-8223/$26.00 © 2011 IEEE

desired magnetic paths while reducing the eddy current loss, the FMPs are made of laminated ferromagnetic material.

Fig. 1(b) shows the topology of the VH machine. There are 6 slots in the inner stator, which are occupied by 3-phase armature windings with 4 poles ($p_s = 2$). Three pole-pairs of PMs are mounted on each stator tooth. The rotor of the VH machine is a slotted rotor with 22 poles.

It should be noted that the overall volumes of these two machines are the same.

III. Mathematical Model

Since the output torque relies on the interaction between the magnetic fields generated by the PMs and the armature windings, the analytical field analysis can provide the designer physical insight into the design criteria of these PMV machines. The time-stepping finite element method is employed to analyze the steady state and transient performance of the PMV machine and VH machine. The core loss calculation method is developed to analyze the iron losses of the machines being studied.

The vector potential distributions in the airspace and slot-opening regions are governed by the Laplace's equation and in the slots and PM (or current carrying regions) regions are governed by the Poisson's equation. So, the problems are described by:

$$\nabla \cdot \left(\upsilon \nabla A - \sigma \frac{\partial A}{\partial t} \right) = \nu \mu_0 \left(\frac{\partial M_x}{\partial y} - \frac{\partial M_y}{\partial x} \right), \quad \text{PM subdomain} \tag{2}$$

$$\nabla \cdot (\upsilon \nabla A) + \frac{d_f N_f}{S_f a p} i_f = 0, \quad \text{stranded windings subdomain} \tag{3}$$

where μ_0 is the permeability of the vacuum; A is the magnetic vector potential; υ is the reluctivity of material and σ is the conductivity; M_x and M_y are the x-y components of the magnetization vector in the PM, respectively; i_f is the winding current; d_f is the polarity (1 or -1) to represent the forward or return path; S_f is the total cross-sectional area of the region occupied by this coil group in the solution domain; N_f is the total conductor number of this winding; a is the number of parallel branches in this winding, and p is the symmetry multiplier which is defined as the ratio of the original full cross-sectional area to the solution area. The no-load electromotive force and electromagnetic torque can be derived from the solution of (2) and (3) which have been thoroughly studied and will not be duplicated here.

The losses of PMV machines consist of the iron loss, friction loss, windage loss and stray loss, in which the iron loss is considered as the major contributor [7]–[9]:

$$P_{hys} = L \int_{\Omega} \left(\frac{1}{T} \int_0^T H_{irr} \cdot dB \right) \tag{6}$$

$$d\Omega = \frac{L}{T} \int_0^T \left(\int_{\Omega} H_{irr} \cdot \frac{dB}{dt} d\Omega \right) dt = \frac{L}{T} \int_0^T \left(\int_{\Omega} \left(H_{irrx} \cdot \frac{dB_x}{dt} + H_{irry} \cdot \frac{dB_y}{dt} \right) d\Omega \right) dt \tag{7}$$

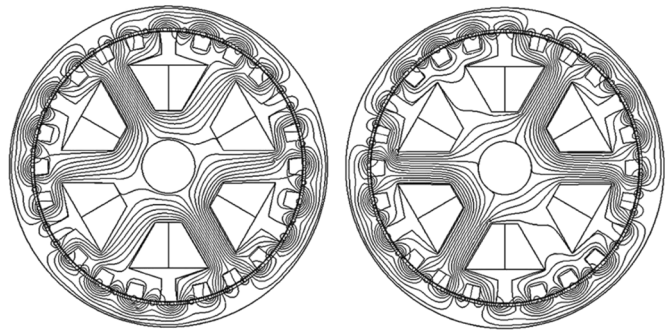

Fig. 2. Magnetic field distributions of PSPMV machine. (a) At 0°. (b) At 90°.

where $\boldsymbol{H}_{\mathrm{irr}}$ is the irreversible component of the magnetic field $\boldsymbol{H}$ and it can be determined according to the iron loss curves with the assumption that the traces of $\boldsymbol{H}_{\mathrm{irr}}$ are elliptical loops. The eddy-current loss in time domain can be deduced as:

$$P_{eddy} = \frac{L}{2\pi^2} \int_{\Omega} \int k_{eddy} \left[\frac{1}{T} \int_0^T \left(\frac{dB}{dt} \right)^2 dt \right] d\Omega = \frac{L}{2\pi^2} \int_{\Omega} \int k_{eddy} \left[\left(\frac{dB_x}{dt} \right)^2 + \left(\frac{dB_y}{dt} \right)^2 \right] d\Omega \tag{8}$$

$$P_{eddy} = \frac{L}{C_{add}} \int_{\Omega} \int k_{add} \left[\left(\frac{dB_x}{dt} \right)^2 + \left(\frac{dB_y}{dt} \right)^2 \right]^{\frac{3}{4}} d\Omega \tag{9}$$

$$C_{add} = (2\pi)^{1.5} \cdot \frac{2}{\pi} \int_0^{\frac{\pi}{2}} (\cos\theta)^{1.5} d\theta \tag{10}$$

where k_{eddy} and k_{add} denote the eddy current loss coefficient and additional loss coefficient, respectively; θ is the angle in polar coordinates of $\boldsymbol{H}_{\mathrm{irr}}$ elliptical loops.

IV. Machine Analysis

A. Performance Comparison

The flux distributions of the PSPMV machine at 0° and 90° are shown in Figs. 2(a) and 2(b), respectively. It can be observed that the flux lines per stator tooth can pass through the FMPs separately, hence verifying the desired flux modulation. It also can be seen that the flux line changes a lot when the rotor rotates one fourth of the rotor pole-pitch. The flux distributions of the VH machine at 0° and 90° are given in Figs. 3(a) and 3(b), respectively. It is noted that the tooth of FMPs in the VH machine are easily saturated.

The corresponding airgap flux density waveforms of the PSPMV machine and VH machine are shown in Figs. 4 and 5, respectively. It can be seen that all of them have 22 pole-pairs in the airgap within 360° which corresponds to 2 pole-pairs of the stator rotating field, thus well agreeing with the principle of vernier machines. Quantitatively, the averaged values of the radial airgap flux density of the PSPMV machine and VH machine are 0.56 T and 0.67 T, respectively. The average values

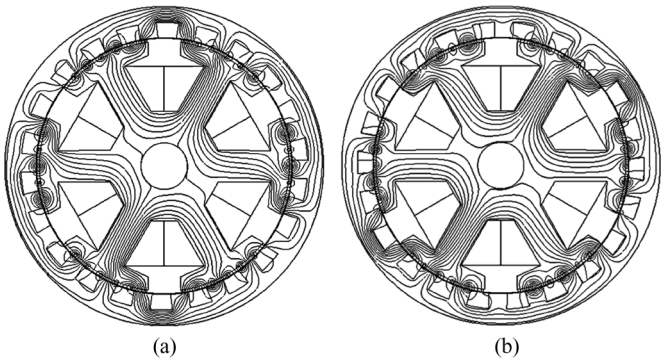

Fig. 3. Magnetic field distributions of VH machine. (a) At 0°. (b) At 90°.

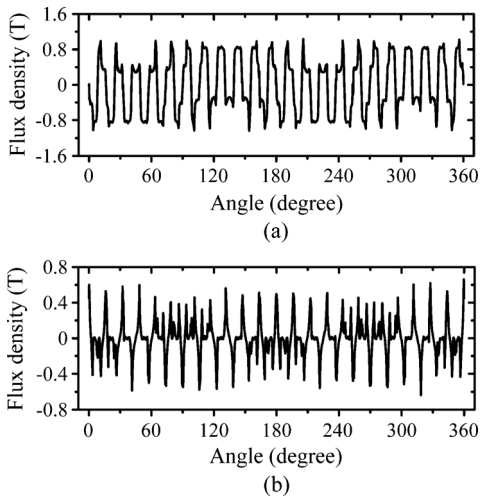

Fig. 4. Airgap flux density waveforms of PSPMV machine. (a) Radial. (b) Tangential.

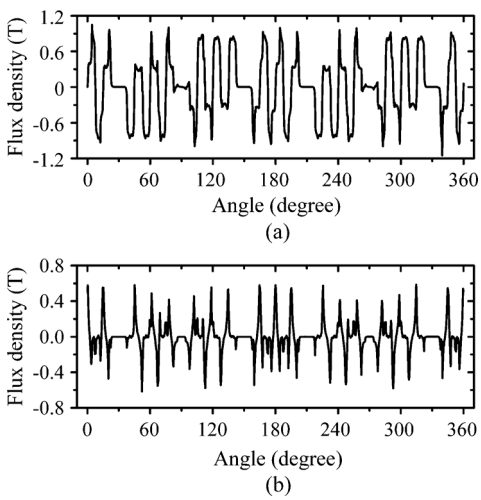

Fig. 5. Airgap flux density waveforms of VH machine. (a) Radial. (b) Tangential.

of the tangential airgap flux density of the PSPMV machine and VH machine are 0.118 T and 0.124 T, respectively.

Fig. 6 shows the no-load electromotive force waveforms of PSPMV machine and VH machine at the rated speed of 300 rpm. It can be found that the root mean square (RMS) values of the PSPMV machine and VH machine are 92.5 V and 86.2 V,

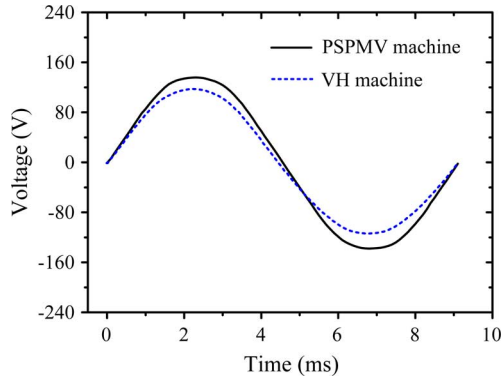

Fig. 6. No-load electromotive force waveforms of PSPMV machine and VH machine.

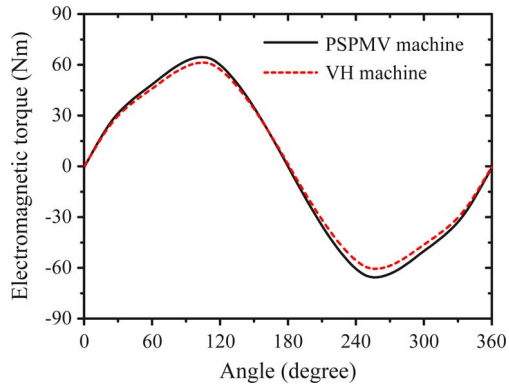

Fig. 7. Electromagnetic torque waveforms of PSPMV machine and VH machine.

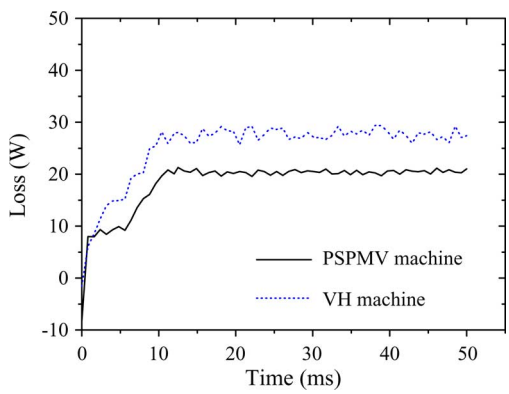

Fig. 8. Core loss waveforms of PSPMV machine and VH machine.

respectively. Namely, the generated voltage of the PSPMV machine is 7.3% higher than that of the VH machine. Moreover, it can be observed that the no-load electromotive force waveforms of the PSPMV machine is very smooth, which is desirable for smooth torque generation.

Furthermore, the torque transmission characteristic is obtained based on the locked-rotor operation. Fig. 7 shows the electromagnetic torque waveforms of the PSPMV machine and VH machine at the rated condition. It can be found that the steady-state torque of the PSPMV machine is 64.9 Nm while the VH machine is 60.9 Nm. Namely, the torque-handling capability of the PSPMV machine is 6.6% higher than that of the VH machine. On the other hand, the torque ripples of

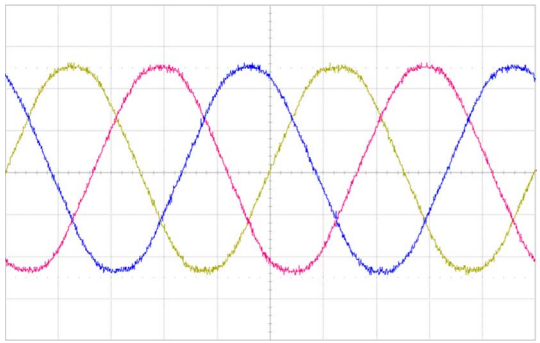

Fig. 9. Measured no-load electromotive force waveforms of PSPMV machine at 300 rpm. (50 V/div, 2 ms/div)

TABLE I
WEIGHT AND COST COMPARISON

Items	PSPMV	VH
Rated power	2 kW	1.9 kW
Rated speed	300 rpm	300 rpm
No. of winding pole-pairs	2	2
No. of FMPs	24	24
No. of rotor pole-pairs/pole	22	22
PM material	NdFeB	NdFeB
Stator and rotor core/FMPs	Laminated steel	Laminated steel
Winding	Copper	Copper
Overall outside diameter	240 mm	240 mm
Shaft diameter	40 mm	40 mm
Axial length	60 mm	60 mm
Airgap length	0.6 mm	0.6 mm
Total copper volume	271 cm^3	271 cm^3
Total iron volume	1748 cm^3	1633 cm^3
Total PM volume	69.6 cm^3	48.4 cm^3
Volume	2714.3 cm^3	2714.3 cm^3
Weight	16.6 kg	15 kg
Cost	\$68.2	\$59.7

the PSPMV machine and VH machine are 5.9% and 5.2%, respectively, mainly due to the cogging torque which occurs at different positions of the stator teeth with different airgap lengths. It should be noted that all these torque ripples are very acceptable. Since the saturation problem is a concern, the core loss curves at no-load of the two machines are shown in Fig. 8. It is shown that the core loss in the PSPMV machine is smaller than that of the VH machine, which is due to the favorable topology of the PSPMV machine. The measured waveforms of the no-load electromotive force of the PSPMV machine at 300 rpm are shown in Fig. 9. It can be observed that the experimental results well agree with the simulation results obtained by using the finite element method.

B. Weight and Cost Comparison

Since the densities of the copper-winding, iron-core and PM materials are 9.0, 7.8 and 7.6 g/cm^3, respectively, the overall weight can be calculated as 16.6 and 15 kg for the PSPMV machine and VH machine respectively. According to the indicative costs of those materials used in the these two machines, namely \$11.2/kg for copper windings, \$1.22/kg for iron cores and \$45.7/kg for PMs, the material cost can readily be deduced from their weights. The overall costs are \$68.2 and \$59.7 for the PSPMV machine and VH machine, respectively. The overall weight and cost comparison of the PSPMV and VH machines are listed in Table I.

It can be found from the results above that the PSPMV machine possesses the larger rated power and higher rated torque for the same machine size and operating frequency. This merit is actually due to the PSPMV structure which can significantly improve its torque density. On the other hand, the required PM materials of the VH machine are less than that of the PSPMV machine, because two pieces of PMs in each the stator slot-opening are saved.

V. CONCLUSION

This paper has presented proposes the comparison of two direct-drive outer-rotor PMV machines, namely the PSPMV machine and VH machine. The generated voltage of the PSPMV machine is 7.3% higher than that of the VH machine. Moreover, it can be observed that the no-load electromotive force waveforms of the PSPMV machine are very smooth, which is desirable for smooth torque generation. The torque-handling capability of the PSPMV machine is 6.6% higher than that of the VH machine. Furthermore, the PSPMV machine possesses the larger rated power and higher rated torque for the same machine size and operating frequency. The overall weight of the VH machine is smaller than that of the PSPMV machine, namely 16.6 kg and 15 kg. The VH machine consumes less PM materials than the PSPMV counterpart. Therefore, the cost of the VH machine is less than that of the PSPMV machine.

REFERENCES

[1] L. Jian and K. T. Chau, "A magnetic-geared outer-rotor permanent-magnet brushless machine for wind power generation," *IEEE Trans. Ind. Appl.*, vol. 45, no. 3, pp. 954–962, 2009.
[2] J. Li and K. T. Chau, "Design and analysis of a HTS vernier PM machine," *IEEE Trans. Appl. Supercond.*, vol. 20, no. 3, pp. 1055–1059, 2010.
[3] A. Toba and T. A. Lipo, "Generic torque-maximizing design methodology of surface permanent-magnet vernier machine," *IEEE Trans. Ind. Appl.*, vol. 36, no. 6, pp. 1539–1546, 2000.
[4] J. G. Li, K. T. Chau, J. Z. Jiang, C. H. Liu, and W. L. Li, "A new efficient permanent-magnet vernier machine for wind power generation," *IEEE Trans. Magn.*, vol. 46, no. 6, pp. 1475–1478, 2010.
[5] E. Spooner and L. Haydock, "Vernier hybrid machines," *Proc. Inst. Electr. Eng.—Electr. Power Appl.*, vol. 150, no. 6, pp. 655–662, 2003.
[6] P. R. M. Brooking and M. A. Mueller, "Power conditioning of the output from a linear vernier hybrid permanent magnet generator for use in direct drive wave energy converters," *Proc. Inst. Electr. Eng.—Generation, Transmission and Distribution*, vol. 152, no. 5, pp. 673–681, 2005.
[7] S. X. Niu, S. L. Ho, W. N. Fu, and L. L. Wang, "Quantitative comparison of novel vernier permanent magnet machines," *IEEE Trans. Magn.*, vol. 46, no. 6, pp. 2032–2035, 2010.
[8] D. Lin, P. Zhou, W. N. Fu, S. Stanton, and Z. J. Cendes, "A dynamic core loss model for soft ferromagnetic and power ferrite materials in transient finite element analysis," *IEEE Trans. Magn.*, vol. 40, no. 2, pp. 1318–1321, 2004.
[9] S. Niu, K. T. Chau, and J. Z. Jiang, "Analysis of eddy-current loss in a double-stator cup-rotor PM machine," *IEEE Trans. Magn.*, vol. 44, no. 11, pp. 4401–4404, 2008.